HHS Public Access

Author manuscript

Nat Neurosci. Author manuscript; available in PMC 2010 January 01.

Published in final edited form as:

Nat Neurosci. 2009 July ; 12(7): 879–887. doi:10.1038/nn.2351.

Regulation of AMPA receptor extrasynaptic insertion by 4.1N, phosphorylation and palmitoylation

Da–Ting Lin[1], **Yuichi Makino**[1], **Kamal Sharma**[1], **Takashi Hayashi**[1], **Rachael Neve**[2], **Kogo Takamiya**[1,3], and **Richard L. Huganir**[1,*]

[1]Department of Neuroscience and Howard Hughes Medical Institute, Johns Hopkins University School of Medicine, 725 N. Wolfe Street, Baltimore, Maryland 21205

[2]MIT / The Picower Institute, 77 Massachusetts Avenue, Cambridge, MA 02139-4307

Abstract

The insertion of alpha–amino–3–hydroxy–5–methyl–4–isoxazolepropionic acid receptors (AMPARs) into the plasma membrane is a key step in synaptic delivery of AMPARs during the expression of synaptic plasticity. However, the molecular mechanisms regulating AMPAR insertion remain elusive. By directly visualizing individual insertion events of the AMPAR subunit GluR1, we demonstrate that Protein 4.1N is required for activity dependent GluR1 insertion. PKC phosphorylation of GluR1 S816 and S818 residues enhances 4.1N binding to GluR1, and facilitates GluR1 insertion. In addition, palmitoylation of GluR1 C811 residue modulates PKC phosphorylation and GluR1 insertion. Finally, disrupting 4.1N dependent GluR1 insertion decreases surface expression of GluR1 and the expression of long–term potentiation (LTP). Our study uncovers a novel mechanism that governs activity dependent GluR1 trafficking, reveals an interesting interplay between AMPAR palmitoylation and phosphorylation, and underscores the functional significance of the 4.1N protein in AMPAR trafficking and synaptic plasticity.

*Corresponding author: Richard L. Huganir, Tel: (410)–955–4050, Email: rhuganir@jhmi.edu.

[3]Current Address: Department of Integrative Physiology, University of Miyazaki Faculty of Medicine, 5200 Kihara Kiyotake Miyazaki, 889–1692, Japan

Author Contributions:

Da–Ting Lin conceived the project, set up the TIRF imaging system, designed and executed majority of experiments, analyzed experimental results and wrote the manuscript.

Yuichi Makino performed *in vivo* virus injection, electrophysiological recordings, and some biochemical experiments, and analyzed experimental results.

Kamal Sharma performed immunocytochemistry studies and analyzed results.

Takashi Hayashi performed ^{3}H–palmitate labeling experiments.

Rachael Neve Provided the HSV expression system.

Kogo Takamiya establishes HSV and lenti–virus system and GluR1 knockout mice.

Richard L. Huganir conceived the project, designed experiments, provided funding and guidance for the project, and wrote the manuscript.

Competing Financial Interests Statement:

Under a licensing agreement between Millipore Corporation and The Johns Hopkins University, R.L.H. is entitled to a share of royalties received by the University on sales of products described in this article. R.L.H. is a paid consultant to Millipore Corporation. The terms of this arrangement are being managed by The Johns Hopkins University in accordance with its conflict–of–interest policies.

Introduction

AMPARs mediate the majority of fast excitatory synaptic transmission in the brain 1, 2. Trafficking of these receptors regulates the number of AMPARs at synapses, and subsequently determines the strength of synaptic transmission 1–3. Activity dependent delivery of AMPARs supplies additional receptors during LTP 4, 5. These AMPARs are thought to originate from recycling endosomes 6, which requires surface insertion of AMPARs. However, the molecular mechanisms governing AMPAR insertion are largely unknown.

Actin filaments are indispensable in maintaining and regulating AMPAR mediated synaptic transmission 7–9. However, the mechanism by which actin cytoskeleton regulates AMPAR trafficking remains elusive. Protein 4.1R is an actin–binding protein that links membrane proteins to the actin cytoskeleton 10, 11. The *Drosophila* 4.1 homolog coracle interacts with GluRA, a homolog of mammalian AMPAR subunit GluR1, but not with GluRB, a homolog of mammalian AMPAR subunit GluR2 12. This interaction is required for synaptic targeting of GluRA 12. 4.1N is a neuronal homolog of 4.1R found in most neurons of adult mouse brain 13. Besides associating with actin cytoskeleton, 4.1N binds specifically to the membrane proximal region (MPR) of GluR1 but not GluR2 14, 15. However, little is known about the functional significance of 4.1N and GluR1 interaction. It is possible that 4.1N regulates AMPAR trafficking by providing a critical link between the actin cytoskeleton and AMPARs.

To examine the molecular mechanisms governing AMPAR trafficking, optical imaging approaches are often employed. These include confocal live imaging 16–21 and sub–resolution particle tracking 22–28. However, these imaging approaches are not well suited for studying AMPAR insertion. Insertion of AMPAR is a dynamic process, and vesicles delivering AMPARs to neuronal surface is likely to contain only limited number of receptors. Such characteristics of AMPAR insertion make its direct visualization difficult, hindering efforts to understand the detailed molecular mechanisms. We employed imaging super–ecliptic pHluorin 29 tagged AMPARs with total internal reflection fluorescence microscopy (TIR–FM) to visualize insertion of AMPARs. By employing such approach, we uncovered a novel mechanism that governs activity dependent GluR1 insertion. Our results underscore the functional significance of activity dependent AMPAR trafficking in synaptic plasticity.

Results

Capturing insertion events of GluRs

TIR–FM offers superior axial resolution, allowing one to image trafficking of receptors near the plasma membrane (∼100nm), and was chosen to achieve direct visualization of AMPAR insertion. To ensure we imaged only surface AMPARs, we chose super–ecliptic pHluorin to label the N–terminus of either GluR1 or GluR2 (R1pH and R2pH, respectively). With this design, the pHluorin tag present in the lumen of transport vesicles and endosomes (pH < 6.0) would be “invisible” to our imaging system and decrease the background signal. Following receptor insertion, the pHluorin tag is exposed to the extracellular space (pH = 7.4) and

undergoes > 20 fold fluorescence increase when the pH changes from < 6.0 to ~ 7.4 29. Therefore, insertion of vesicles containing pHluorin labeled AMPAR would significantly increase pHluorin fluorescence 18–21.

By imaging pHluorin labeled AMPARs under TIR–FM, we were able to visualize rapid appearance of surface R1pH clusters (Fig. 1a and Movie S1). R1pH insertion could also be observed under epi–fluorescent illumination, under which condition pre–existing synaptic R1pH puncta were clearly visible (Fig. 1b). We could observe insertion events in both soma and dendritic shafts but never in dendritic spines (Fig. 1b). Insertion events appeared as the rapid appearance of R1pH clusters that then quickly dispersed within seconds (Fig. 1c and Movie S1–Movie S3). We also observed lateral diffusion of R1pH following insertion in both somatic (Fig. S1) and dendritic surface (Fig. 1c and S2 and Movie S3). Diffusion of inserted R1pH into adjacent spines could also be observed (Fig. S2). The insertion events can be visualized graphically in space and time by generating a y–t rendering image (Fig. 2a and Movie S2). Two possibilities can account for the dynamic appearance of R1pH clusters, insertion of R1pH from intracellular compartments, or clustering of pre–existing surface R1pH. We reasoned that if the observed cluster was the accumulation of pre–existing surface R1pH, photo–bleaching pre–existing R1pH fluorescence should significantly reduce both the intensity and the frequency of these clusters. Conversely, if the observed clusters were to represent R1pH insertion, photo–bleaching pre–existing surface R1pH should have minimal effect on these R1pH clusters, since intracellular “invisible” pools of R1pH are protected from photo–bleach 19. Photo–bleaching pre–existing surface R1pH reduced neither the amplitude nor the frequency of subsequent R1pH clusters (Fig. S3). Furthermore, we could abolish the appearance of these clusters either by bath application of Botulinum toxin A treatment, or by co–transfection of tetanus toxin light chain expression vector with R1pH (Fig. 2b). Together, these data demonstrate that the observed appearance of R1pH clusters represents insertion events.

GluR1 has often been implicated in activity dependent AMPAR trafficking while GluR2 has been more closely associated with constitutive AMPAR trafficking 30. Acute suppression of excitatory neuronal activity by applying a cocktail of TTX (1 μM), NBQX (20 μM) and DL–APV (200 μM) significantly reduced the insertion frequency of R1pH (Fig. 2b). In addition, we rarely observed R2pH insertion under normal conditions (Fig. 2b). Furthermore, co–expressing non–tagged GluR2 with R1pH does not affect R1pH insertion, while co–expressing non–tagged GluR1 with R2pH significantly increased R2pH insertion (Fig. 2b), indicating that GluR1 dominates over GluR2 in heteromeric AMPARs. We conclude that we can directly visualize activity dependent GluR1 insertion only in the extrasynaptic surface.

4.1N is required for GluR1 insertion

To further examine molecular mechanisms governing GluR1 insertion, we generated several C–terminal deletions of R1pH: R1pH(1–880) that lacked PDZ ligand of GluR1; R1pH(1–833) that lacked the S845 phosphorylation site yet retained the S831 phosphorylation site; R1pH(1–822) that still contained GluR1 MPR; and R1pH(1–814) that lacked majority of GluR1 C–terminus (Fig. 3a). Using our TIRF imaging approach, we found no significant differences between the insertion frequencies of R1pH(1–880), R1pH(1–833), and R1pH(1–

822) and that of R1pH (Fig. 3b,c). However, we observed significantly reduced insertion frequency with R1pH(1–814) (Fig. 3b,c]. The distinction between R1pH(1–814) and R1pH(1–822) was that the GluR1 MPR was deleted in R1pH(1–814) (Fig. 3a), suggesting that the GluR1 MPR plays an important role in GluR1 insertion.

The GluR1 MPR is required for binding of GluR1 to 4.1N 15. To test the function of 4.1N in GluR1 insertion, we first generated a GluR1 deletion mutant (R1pHΔ808–822) that lacked only the MPR. We observed significantly reduced insertion frequency with R1pHΔ808–822 (Fig. 4a,b). Conversely, co–expressing 4.1N with R1pH significantly increased the insertion frequency of GluR1. In contrast, this effect of 4.1N over–expression was abolished when 4.1N was co–expressed with R1pHΔ808–822 (Fig. 4a,b). Together, these results indicate that direct interaction between 4.1N and GluR1 MPR is required for GluR1 insertion. To test this hypothesis, we examined GluR1 insertion when 4.1N expression level was knocked down using RNA interference (RNAi). We first tested the effect of a pool of 4 small interference RNA (siRNA) targeting rat 4.1N. In young neurons, this siRNA pool was able to reduce protein expression level of endogenous 4.1N compared to control non–targeting siRNA (Fig. 4c). Co–transfecting this siRNA pool with R1pH significantly reduced R1pH insertion frequency (Fig. 4a,b). Based on the sequences of the 4.1N siRNA pool, we generated 3 short hairpin RNAs (shRNA) in both pSuper and lentiviral vectors (see Methods), one of which (#11) was able to knock down the expression level of endogenous rat 4.1N protein by 80% (Fig. 4c). Based on the sequence of 4.1N shRNA#11, a rescue construct of 4.1N was generated in both pRK5 and Herpes simplex virus (HSV) vector. The HSV version of this construct was able to rescue the expression of 4.1N in the presence of lentivirus shRNA#11 in cultured neurons (Fig. 4c). We next used plasmid–based shRNA and rescue constructs to further examine the role of 4.1N in GluR1 insertion. 4.1N shRNA#11 significantly reduced GluR1 insertion frequency, while the rescue construct of 4.1N enhanced insertion frequency of GluR1 in the presence of shRNA#11 (Fig. 4a,b). These results demonstrate that 4.1N is critical for GluR1 insertion.

Post–translational modifications regulate GluR1 insertion

Within the GluR1 MPR, the serine 818 (S818) is a PKC phosphorylation site (Fig. 5a) 31. The presence of this PKC phosphorylation sites within the GluR1 MPR raises the possibility that PKC may regulate GluR1 insertion. Go 6983, a broad spectrum PKC inhibitor, significantly reduced GluR1 insertion (Fig. 5b,c), whereas phorbol 12–myristate 13–acetate (PMA), a PKC activator, significantly increased GluR1 insertion (Fig. 5b,c). These results demonstrate that manipulating PKC activity bi–directionally regulates GluR1 insertion. The only difference between the MPR of GluR1 and GluR2 is that serine 816 and 818 in GluR1 are replaced with alanine in GluR2 (Fig. 5a). We hypothesize that phosphorylation of these two serine residues may regulate GluR1 insertion. To test this hypothesis, we generated and tested R1pH carrying single or double mutations of S816 and S818 using TIRF imaging. We generated serine to alanine mutations to abolish phosphorylation and serine to aspartate mutations to mimic phosphorylation of these serine residues. The insertion of the single serine to alanine point mutations, R1pHS816A or R1pHS818A, was not significantly different from that of R1pH (Fig. 5b,c). However, the double serine to alanine point mutations, R1pHS816A,S818A, displayed significantly lower insertion frequency (Fig.

5b,c). These results demonstrate that the presence of serine residues at either 816 or 818 positions is able to maintain basal level of GluR1 insertion, but without both serine residues, GluR1 insertion is abolished. These results suggest that phosphorylation of these serine residues may affect GluR1 insertion. Mimicking phosphorylation of both S816 and S818 (R1pHS816D,S818D) significantly increased insertion frequency of GluR1, whereas neither R1pHS816D nor R1pHS818D increased insertion frequency of GluR1 (Fig. 5b,c). These results suggest that phosphorylation of both S816 and S818 is required to enhance GluR1 insertion. The phosphorylation of these two serine residues is mediated by PKC, since GluR1S816A,S818A abolished the effect of PMA in enhancing GluR1 insertion (Fig. 5b,c). This phosphorylation is likely to regulate 4.1N and GluR1 interaction, since GluR1S816A,S818A also abolished the effect of 4.1N in enhancing GluR1 insertion (Fig. 5b,c). Although phosphorylation of both S816 and S818 was required to enhance GluR1 insertion, it is not sufficient to enhance GluR1 insertion, since Go 6893 also efficiently reduced insertion frequency of R1pHS816D,S818D (Fig. 5b,c). This result suggests that in addition to phosphorylation of GluR1 S816 and S818, other PKC dependent signaling events are also required for GluR1 insertion. Together, our results demonstrate that phosphorylation of GluR1 S816 and S818 play a critical role in regulating activity dependent GluR1 insertion, potentially by affecting the interaction between 4.1N and GluR1.

In the proximity of the S816 and S818 residues within the GluR1 MPR, the C811 residue is palmitoylated 32. Moreover, the interaction between 4.1N and GluR1 is regulated by the palmitoylation state of the C811 residue 32, but the significance of this regulation is unclear. Interestingly, the palmitoylation deficient mutant of GluR1, GluR1C811S, also demonstrated increased insertion frequency (Fig. 5b,c), suggesting that palmitoylation of GluR1 C811 residue regulates GluR1 insertion by regulating 4.1N and GluR1 interaction. The proximity between the palmitoylation site and the phosphorylation sites indicates a potential interplay between palmitoylation and phosphorylation within the GluR1 MPR (Fig. 5a). We reason that if phosphorylation regulates palmitoylation within the GluR1 MPR, mimicking de–palmitoylation state of the C811 residue with GluR1C811S should rescue reduced insertion of GluR1S816A,S818A. Conversely, if de–palmitoylation regulates phosphorylation within the GluR1 MPR, abolishing phosphorylation with GluR1S816A,S818A should block the enhanced insertion of GluR1C811S. However, if there is no interplay between palmitoylation and phosphorylation, combining C811S with S816DS818D should have additive affects on GluR1 insertion. Our results showed that the insertion frequency of R1pHC811S,S816A,S818A was similar to that of R1pHS816A,S818A, whereas the insertion frequency of R1pHC811S,S816D,S818D was similar to that of R1pHS816D,S818D (Fig. 5b,c). These results demonstrate that the phosphorylation state of both S816 and S818 bypasses the effect of de–palmitoylation at C811, and suggest that de–palmitoylation of the C811 residue regulates phosphorylation at both S816 and S818 residues, a signaling event that likely affects the interaction between 4.1N and GluR1.

Regulation of 4.1N and GluR1 interaction

4.1N binds directly to GluR1 both *in vitro* and *in vivo* 15. We first confirmed the interaction between endogenous 4.1N and GluR1 in cultured neurons using co–immuno–precipitation

(co–IP) approach (Fig. S4). The interaction between endogenous 4.1N and GluR1 was significantly reduced by Go 6983 and enhanced by PMA (Fig. 6a,b). To further examine whether phosphorylation and palmitoylation of GluR1 MPR regulated 4.1N and GluR1 interaction, neurons were cultured from GluR1 knockout mice, and various myc–tagged GluR1 constructs were expressed in these neurons using the HSV expression system. Co–IP of endogenous 4.1N with virally expressed myc–tagged GluR1 was used to examine the interaction between these two proteins. Without rescuing the expression of GluR1, 4.1N was absent from the IP complex, demonstrating the specificity of our approach (Fig. 6c). Following rescuing GluR1 expression, the interaction between endogenous 4.1N and virally expressed myc–GluR1 was apparent (Fig. 6c). Mutation of S816A and S818A (myc–GluR1S816A,S818A) abolished the interaction between GluR1 and 4.1N (Fig. 6c,d). Conversely, the binding of 4.1N to the phosphomimetic mutant (myc–GluR1S816D,S818D) was stronger than to myc–GluR1 (Fig. 6c,d). This result demonstrates that phosphorylation of both S816 and S818 residues regulate 4.1N and GluR1 interaction. In addition, the interaction between 4.1N and the palmitoylation mutant myc–GluR1C811S was also enhanced (Fig. 6c,d), consistent with previous results from our laboratory 32. Moreover, the interaction between 4.1N and myc–GluR1C811S,S816A,S818A was also abolished (Fig. 6c,d), suggesting again that the effect of de–palmitoylation at C811 residue requires the presence of serine residues at both 816 and 818 positions. The interaction between 4.1N and myc–GluR1C811S,S816D,S818D was similar to that between 4.1N and myc–GluR1S816S,S818D (Fig. 6c,d). Together, these results suggest that de–palmitoylation of GluR1C811 residue enhances the interaction between 4.1N and GluR1 by facilitating phosphorylation at S816 and S818 residues.

To further test this hypothesis, we examined how mimicking the de–palmitoylation state of the C811 residue might affect PKC phosphorylation at the S818 residue 31. Change in the phosphorylation level of S818 residue was examined using a previously characterized anti–GluR1 phospho–S818 antibody 31. This antibody could detect a clear signal that was sensitive to λ phosphatase treatment (Fig. 6e), while the signal detected by anti–GluR1 N–terminus antibody was un–affected (Fig. 6e), confirming the specificity of our anti–GluR1 phospho–S818 antibody 31. Following PKC activation, the phosphorylation level of S818 residue detected by this antibody was higher in GluR1C811S compared to that of GluR1 (Fig. 6e,f). This result demonstrates that mimicking de–palmitoylation state of the C811 residue could enhance phosphorylation of S818 residue by PKC. However, the phosphorylation state of GluR1 S816 and S818 residues did not affect palmitoylation of GluR1 C811 residue (Fig. S5). Together, our data suggest that de–palmitoylation of the C811 residue facilitates phosphorylation within GluR1 MPR by PKC, which in turn enhances the interaction between 4.1N and GluR1.

Functional significance of GluR1 insertion

To investigate the functional significance of activity dependent GluR1 insertion, we first examined steady state GluR1 surface expression under conditions of altered GluR1 insertion. We cultured neurons from GluR1 knockout mice, and rescued GluR1 (non–tagged) expression using HSV to examine surface expression of various GluR1 mutants. GluR1(1–822), a deletion mutant that did not display a defect in insertion frequency, showed

similar surface expression compared to GluR1 (Fig. 7a,b). GluR1(1–814), GluR1S816A,S818A, as well as GluR1C811S,S816A,S818A, all of which showed significant reduction in insertion frequency, demonstrated 30–40% reduction in surface expression (Fig. 7a,b). These results suggest that activity dependent GluR1 insertion is required to maintain steady state surface expression of GluR1. Interestingly, We observed > 80% reduction in steady state surface level with GluR1Δ808–822 (Fig. 7a,b), likely due to elimination of 4.1N binding by deleting the MPR region and incomplete elimination of 4.1N binding by the serine mutations. In addition, we did not observe significant changes in either the patterns or the levels of expression of different GluR1 constructs used in our experiments (Fig. S6 and S7). However, the surface expression of GluR1S816D,S818D, GluR1C811S, and GluR1C811S,S816D,S818D were not significantly different from that of GluR1 (Fig. 7a,b), even though these mutants displayed significantly increased insertion. These results suggest that simply increasing activity dependent GluR1 insertion does not affect steady state surface expression of GluR1, possibly due to the lack of other mechanisms to stabilize inserted receptors on the neuronal surface or to other compensatory effects on receptor trafficking. Finally, surface expression of endogenous GluR1 containing AMPARs was significantly reduced when we knocked down 4.1N using siRNA (Fig. 7c). Together, these data demonstrate that disrupting 4.1N and GluR1 interaction and activity dependent GluR1 insertion over a prolonged period of time reduces steady state surface expression of GluR1, leading to disruption of GluR1 trafficking.

To investigate the functional significance of 4.1N and GluR1 interaction in synaptic plasticity, we turn to the well–characterized synaptic plasticity paradigm, hippocampal Schaffer collateral – CA1 LTP. We identified a lentiviral based 4.1N shRNA construct that could efficiently knock down endogenous mouse 4.1N in dissociated cultured neurons (Fig. 8a). *In vivo* injection of this virus specifically into hippocampus CA1 region could also efficiently knock down the expression of endogenous 4.1N (Fig. 8a,b). We prepared acute hippocampal slices from 6–week old mice injected with lentivirus one week earlier, and obtained whole cell recording from infected or non–infected CA1 pyramidal neurons. We measured basal synaptic responses using the ratio between AMPAR mediated current and N-methyl-D-aspartic acid (NMDA) receptor mediated current (AMPA/NMDA ratio). The AMPA/NMDA ratio from 4.1N knockdown neurons was not significantly different from that of either uninfected neurons or lenti–GFP infected neurons (Fig. 8c). In contrast, knocking down 4.1N significantly reduced LTP expression 50–60 minutes after induction (Fig. 8d), without affecting the initial phase (up to 30 minutes after induction) of LTP expression. Lentivirus expressing either GFP or a control non-targeting shRNA had no effect on LTP expression. These results suggest that 4.1N plays an important role in the expression of LTP without affecting basal synaptic transmission. A recent work showed that knocking out both 4.1N and 4.1G affected neither basal synaptic transmission nor synaptic plasticity in 3–week old mice 33. Since our LTP experiments were performed with 6–week old mice and used acute knockdown of 4.1N, the difference in LTP results may be due to the age difference of mice used, and/or that acute knockdown of 4.1N minimizes potential developmental compensatory mechanisms.

Discussion

Insertion of AMPARs to the neuronal surface is one of the key steps in the synaptic delivery of AMPARs. By imaging super–ecliptic pHluorin tagged AMPARs under TIR–FM, we were able to capture individual GluR1 insertion events. Similar insertion events could also be observed under epi–fluorescent illumination mode, under which condition synaptic populations of GluR1 are visible. We observed GluR1 insertion only on extra–synaptic surfaces of both soma and dendritic shaft, and fail to observe GluR1 insertion on spines. Similar GluR1 insertions were reported recently using the same approach 34. The authors reported that the GluR1 insertions they observed were extra–synaptic, and that chemically mimicking "LTP" stimulation results in an increase in GluR1 insertion frequency but not the contents of individual vesicles 34. The observation of extra–synaptic insertion of GluR1, together with a series of elegant studies demonstrating the importance of lateral diffusion in supplying AMPARs to synapses 22–28, supports a two–step mechanism for synaptic delivery of AMPAR: an extra–synaptic insertion step, and a subsequent step involving lateral diffusion from extra–synaptic pools. Such a two–step synaptic delivery of AMPARs to synapses has been shown to occur in the induction of calcium–permeable AMPA receptor plasticity (CARP) in cerebellar parallel fiber – stellate cell synapse 35, 36. Our data also underscore the importance of maintaining an extra–synaptic surface pool of AMPARs. Maintaining the size of this pool through regulating activity dependent AMPAR insertion is likely to ensure AMPAR supply to synapses during high neuronal activity, and provide a pool for recruitment of AMPARs to synapses during LTP.

Phosphorylation of AMPARs plays an important role in AMPAR trafficking and synaptic plasticity 18, 19, 31, 37–42. Phosphorylation affects AMPAR trafficking most likely through regulating the interaction between AMPARs and their binding partners. For example, phosphorylation of GluR2 S880 residue differentially regulates binding of PICK1 or GRIP to GluR2 43. However, for most other AMPAR phosphorylation sites, such binding partners of AMPARs remain unknown. Identifying these binding partners would significantly contribute to understanding the mechanisms by which phosphorylation regulate AMPAR trafficking and synaptic plasticity. Here we identified 4.1N as such a phosphorylation dependent binding partner to GluR1. We showed that phosphorylation of serine residues on the GluR1 MPR enhanced 4.1N and GluR1 interaction, which in turn enhanced activity dependent GluR1 insertion to surface extra–synaptic pools. The extra–synaptic pools of AMPARs may serve as a source of AMPARs for delivery to synapses during LTP. And replenishing these extrasynaptic AMPAR pools would be important for the maintenance of LTP. Consequently, a deficit in activity dependent AMPAR insertion would fail to maintain the expression of LTP without affecting the initial phase of expression. Such pattern of LTP expression was observed when 4.1N was knocked down, and was also observed by the blocking GluR1 S818 phosphorylation 31. These results suggest that phosphorylation of GluR1 S818 facilitates LTP expression by enhancing 4.1N and GluR1 interaction, and that 4.1N regulates GluR1 insertion to maintain an extrasynaptic pool of GluR1, which is required to sustain the synaptic potentiation through supplying AMPARs to synapses.

Besides phosphorylation, palmitoylation is also known to regulate both synaptic function and AMPAR trafficking 32, 44–49. However, the detailed molecular mechanism by which palmitoylation of GluR1 C811 residue regulates GluR1 trafficking was unclear. Our data revealed that de–palmitoylation of GluR1 C811 residue led to PKC phosphorylation within its proximity, which in turn enhanced the interaction between 4.1N and GluR1 and resulted in increased GluR1 insertion. Regulation of PKA phosphorylation of the β_2–adrenergic receptor by palmitoylation has been reported 50. This is achieved through restricting access of the phosphorylation site to PKA by palmitoylation 50. Our results suggest that palmitoylation of GluR1 C811 residue employs a similar mechanism to restrict PKC phosphorylation of the S816 and S818 residues. Our results further suggest that such interplay between protein palmitoylation and phosphorylation may be a more general mechanism governing receptor trafficking.

In summary, by directly visualizing GluR1 insertion, we uncovered a novel molecular mechanism governing activity dependent GluR1 insertion (Fig. S8). Such a mechanism contributes to maintaining normal levels of surface AMPARs, and play an important role in ensuring extrasynaptic pools of AMPARs for recruitment to synapses during LTP.

Methods

Molecular Biology

All restriction enzymes were from New England BioLabs (Ipswich, MA). Chemicals were from Thermo Fisher Scientific (Waltham, MA). TTX, NBQX, APV, Go 6983, and PMA were from Tocris Bioscience (Ellisville, Missouri). DNA Sequencing was performed at the JHUSOM Sequencing Facility.

RNA Interference (RNAi)

ON–TARGETplus SMARTPool siRNAs was obtained from Dharmacon (Lafayette, CO): Cat# J–092240–09; J–092240–10; J–092240–11; J–092240–12.

To generate shRNAs targeting rat 4.1N in pSuper vector, oligos derived from sequences provided by Dharmacon were annealed and directly subcloned into pSuper vector (Oligoengine, Inc., Seattle, Wa) between Bgl II and Xho I sites. The oligo sequence for different shRNAs were as following:

4.1N shRNA#9

Sense:GATCCCCAGACGGTGGCCACGGAAATTTCAAGAGAATTTCCGTGGCCACC GTCTTTTTTTC

Antisense:TCGAGAAAAAAAGACGGTGGCCACGGAAATTCTCTTGAAATTTCCGTG G CCACCGTCTGGG

4.1N shRNA#10

Sense:GATCCCCGGGATGAAGATGTCGATCATTCAAGAGATGATCGACATCTTCA T CCCTTTTTTC

Antisense:TCGAGAAAAAAGGGATGAAGATGTCGATCATCTCTTGAATGATCGAC AT CTTCATCCCGGG

4.1N shRNA#11

Sense:GATCCCCAGGAGAGGGATGCGGTATTTTCAAGAGAAATACCGCATCCCTC T CCTTTTTTTC

Antisense:TCGAGAAAAAAAGGAGAGGGATGCGGTATTTCTCTTGAAAATACCGC AT CCCTCTCCTGGG

Scrambled shRNA:

Sense:GATCCCCGCGCGCTTTGTAGGATTCGTTCAAGAGACGAATCCTACAAAGC G CGCTTTTTTC

Antisense:TCGAGAAAAAAGCGCGCTTTGTAGGATTCGTCTCTTGAACGAATCCTA C AAAGCGCGCGGG

To generated lentiviral based shRNA constructs, the H–1 promoter and the shRNA sequences in pSuper were amplified by PCR and subcloned into the Pac I site of the lentiviral vector FUGW. Rat hippocampal or cortical cultured neurons were infected with different lentivirus at DIV5, and harvested for western blot at DIV12. 4.1N were detected with monoclonal anti–4.1N antibody (Cat# 611836, BD Biosciences, San Jose, CA). A 4.1N rescue construct was also generated based on shRNA#11 (final sequence within the target region was: AAGAACGAGACGCCGTGTT, underlined nucleotides were the mismatches within target region). This 4.1N rescue construct was subcloned into both pRK5 and HSV1005(+) vectors. To verify that this rescue construct was not targeted by 4.1N shRNA#11, we infected hippocampal neurons with lentivirus 4.1N shRNA#11 at DIV5. At DIV10, these neurons were then infected with HSV–4.1N rescue construct. Neurons were harvested at DIV12 for western blot. The target sequence of shRNA#10 was identical between mouse and rat, and lentiviral shRNA#10 was able to knock down endogenous mouse 4.1N by > 80%. This construct was chosen for all the experiments involving knock down of mouse 4.1N protein.

Neuronal Culture

Hippocampal neurons from embryonic day 18 (E18) rats were seeded on 25 mm coverslips (size #1.5) pre–coated with poly–L–Lysine (0.1M in Borate Buffer, pH = 8.0). The plating media were Neurobasal media containing P/S/G (50 U/mL Penicillin, 50 μg/mL Streptomycin, 2 mM Glutamax) supplemented with 2% B–27 and 5% fetal bovine serum (FBS) (Invitrogen, Carlsbad, CA). 24 hours after plating, neurons were switched to feeding media (plating medium without FBS) and maintained in serum free conditions thereafter. Mice cortical neurons were seeded on poly–L–Lysine coated dishes in plating media. After 24 hours, neurons were switched to fresh plating media in order to remove any debris from initial seeding. Neurons were then fed twice a week with feeding media.

HSV Production

All the HSV constructs were generated in HSV vector HSV1005(+). Replication deficient HSV were produced using 5*dl*1.2 helper virus and 2–2 cells (see Current Protocols in Neuroscience 4.13). 2–2 cells were maintained in DMEM media containing P/S/G supplemented with 10% FBS. 2–2 cells were transfected with HSV vectors using LipofectAmine2000 (Invitrogen, Carlsbad, CA). 24 hours after transfection, 2–2 cells were switched to DMEM containing 2% FBS, and 5*dl*1.2 helper virus was added. 48 hours after helper virus infection, cells were harvested and subjected to 3 cycles of freeze/thaw, followed by sonication in a water bath sonicator. Supernatant of cell lysate containing the P0 virus was collected and used to re–infected 2–2 cells. The infection / harvest cycle was repeated 3 times, and the final P3 virus were purified in sucrose gradient, re–suspended in 10% sucrose solution and stored at –80°C until use.

Lentivirus Production

Lentivirus was produced in HEK293T cells using the FUW / Δ8.9 / VSVG system (5 μg, 3.75 μg.9, and 2.5 μg respectively for each 10 cm dish). Cells were maintained with DMEM containing P/S/G. 48 hours after transfection, culture media were collected and fresh media were added to the transfected cells and collected 24 hours later again. The two collections of media were combined and virus particles were pelleted by ultra–centrifugation (25,000 rpm, Beckman SW 28 rotor). Virus particles were then re–suspended with Neurobasal media and stored at –80°C until use.

Surface Biotinylation

Neurons were rinsed with cold ACSF (in mM: 119 NaCl, 2.5 KCl, 2 $CaCl_2$, 1 $MgCl_2$, 25 HEPES, pH = 7.4 and 30 D–Glucose) and incubated with ACSF containing 1.5 mg/mL sulfo–NHS–SS–biotin (Thermo Fisher Scientific Inc., Waltham, MA) for 20 minutes at 10°C. Neurons were subsequently washed with cold ACSF, and incubated with ACSF plus 50 mM glycine to quench un–reacted biotin. Neurons were then scraped into ice–cold lysis buffer (25 mM Tris, pH 7.4, 1.5% Triton X–100, 250 mM NaCl, 5mM EDTA, 5mM EGTA, 50mM NaF, 5mM NaPPi , protease inhibitor cocktail). A small fraction of supernatant was collected to detect total level of GluR1, and the remaining supernatant was incubated with Ultralink–neutravidin (Thermo Fisher Scientific Inc., Waltham, MA) beads for 3 hours to isolate biotinylated proteins. Both the total and biotinylated proteins were subjected to SDS–PAGE and detected using monoclonal anti–GluR1 N–terminus antibody (clone 007.4.9D, Huganir Lab). Western Blots were performed using the SNAP i.d. system (Millipore). The ratio of surface/total of each sample was normalized to GluR1 wild type as 100%.

Immunoprecipitation

Neurons were solubilized with lysis buffer as mentioned above. To detect GluR1 S818 phosphorylation, polyclonal anti–GluR1 C–terminus antibody (JH4294) was used for immunoprecipitation. To detect association of endogenous 4.1N with GluR1, anti–GluR1 N–terminus polyclonal antibody (JH5871) was used to avoid any potential interference of 4.1N and GluR1 interaction by antibody. To detect association between different virally expressed myc–tagged GluR1 constructs and endogenous 4.1N, anti–myc antibody (clone

9E10) were used. IP reaction was performed in lysis buffer for 3 hours, followed by 5 washes in lysis buffer containing 500 mM NaCl. Samples were separated by 7.5% SDS–PAGE. GluR1 was detected using the monoclonal anti–GluR1 N–terminus antibody and 4.1N was detected by monoclonal anti 4.1N antibody (BD Bioscience).

Immuno–labeling of surface GluR1

Hippocampal neurons were incubated with polyclonal anti–GluR1 N–terminal antibody (JH1816) for 20 minutes at 10°C, fixed with Parafix (4% Sucrose, 4% para–formaldehyde in PBS), and subsequently stained with fluorescently labeled secondary antibody and mounted on slides. Images were acquired on a Zeiss LSM 510 using a 63× objective (N.A. = 1.40). Fluorescent intensities were quantified using ImageJ [Rasband, W.S., NIH, http://rsb.info.nih.gov/ij/, 1997–2007]. Total surface GluR1 signal of transfected neurons was normalized to neighboring non–transfected neurons as 100%.

TIRF Imaging

The TIRF imaging system was based on a manual Zeiss AxioObserver microscope (Carl Zeiss MicroImaging, Inc., Thornwood, NY). The excitation laser was a Coherent Sapphire 488–50mW (OEM version, Coherent Inc., Santa Clara, CA). Laser was coupled to a Zeiss TIRF slider via a KineFLEX–P–2–S–488–640–0.7–FCP–P2 fiber optics (Point Source, Mitchell Point, Hamble, UK). A Z488RDC dichroic mirror (Chroma Technology Corporation, Rockingham, VT) was used to reflect the incoming laser onto a Zeiss α–plan 100X objective (N.A. = 1.45, Carl Zeiss). An ET525/50 emission filter was used for GFP fluorescence detection (Chroma Technology Corporation). An EMCCD camera (ImagEM C9100-13, Hamamatsu) was used as detector. The camera was maintained at –80°C during experiment using a JULABO HF25-ED heating and refrigerated circulator (JD Instruments, Inc.). A Uniblitz LS6 shutter controlled by VCM–D1 (Vincent Associates) was integrated between the laser head and the fiber launcher. Data were acquired using Zeiss AxioVision software (Carl Zeiss). Neurons between the ages of DIV12-15 were used for imaging experiments. All the imaging experiments were performed in ACSF solutions at room temperature (23–25 °C). Imaging exposure was adjusted such that image acquisition rate is 10 images per second (10 Hz). To increase the signal to noise ratio, we typically performed 1 minute photo–bleach before data acquisition. Recordings were analyzed using ImageJ, and insertion events lasting longer than 1 second were registered as an event manually. Total events per minute were taken as the frequency of insertion. Y–t rendering images were generated by rotating the original x–y–t stack 90° along y–axis, and the maximum intensity of each x line was projected onto a single pixel of y axis using maximum intensity projection algorithm. To generate composite images indicating the site of insertion as shown in Figure 1, the maximum intensity of x–y–t stack was projected along the t axis to generate a mask that indicates the site of insertion. The final RGB composite images were generated by merging the neuronal morphology image as magenta and the mask image for insertion site as green using ImageJ.

In vivo Injection of Lentivirus

Five to six week old C57BL/6 mice were anesthetized with intraperitoneal injection of avertin (tribromoethanol, 0.25 mg/g body weight; 2–methyl–2–butanol, 0.16 μl/g body

weight) and mannitol (to prevent edema, 10 mg/g body weight). After immobilizing mouse on a stereotaxic instrument, we exposed mouse skull and drilled a small hole above the hippocampus of each hemisphere. Viral solution was prepared in a glass pipette (tip diameter of 20–30 μm). Viral solution was injected to 8 different sites of CA1 per hemisphere consisting of 4 horizontal locations (around ∼2.5 mm posterior and ∼2.0 mm lateral to bregma, ∼0.5 mm away from each other) at 2 different depths (1.2 mm and 1.4 mm ventral to the surface of cortex). Injection lasted 5 min per site at a flow rate of 0.15 μl/min. Buprenorphin (0.06 mg/g body weight) was injected subcutaneously following injection for analgesia. All experiments were done in accordance with the policies of the Animal Care and Use Committee of the Johns Hopkins University School of Medicine.

Hippocampal slice preparation

Acute hippocampal slices were prepared 1 week after virus injection. Mice were anesthetized with intraperitoneal injection of avertin, and intracardiac perfused with ice–cold cutting solution (in mM: 119 Choline Cl, 2.5 KCl, 7.0 $MgSO_4$, 1.0 $CaCl_2$, 1.0 NaH_2PO_4, 26 $NaHCO_3$, 1.0 kynurenic acid, 1.3 Na–ascorbate, 3.0 Na–pyruvate, 30 glucose, saturated with 95% O_2 / 5% CO_2). Mouse brain was removed rapidly and placed in ice–cold cutting solution. Coronal slices (300 μm thick) were prepared with vibratome (Leica VT1200S). Slices were recovered in aCSF (in mM: 119 NaCl, 2.5 KCl, 1.3 $MgSO_4$, 2.5 $CaCl_2$, 1.0 NaH_2PO_4, 26 $NaHCO_3$, 11 glucose, oxygenated with 95% O_2 / 5% CO_2) supplemented with 1.0 mM kynurenic acid at 35 °C for 1 hour then kept in aCSF at room temperature until recordings.

Whole–cell recordings

Slices were placed in a submerged chamber and perfused with aCSF supplemented with 100 μM picrotoxin, 10 μM glycine, 2.7 mM $MgSO_4$ (total 4.0 mM) and 1.5 mM $CaCl_2$ (total 4.0 mM) at room temperature. Whole–cell recordings were obtained from CA1 pyramidal cells under DIC and fluorescent illumination. Intracellular solution contained (in mM) 115 $CsMeSO_4$, 0.4 EGTA, 5.0 TEA–Cl, 2.8 NaCl, 20 HEPES, 3.0 MgATP, 0.5 GTP, 10 Na_2 phosphocreatine, pH = 7.2 and osmolality 285–290 mOsm. A multiclamp 700A amplifier (Axon Instruments) was used for acquisition. Signals were digitized at 10 kHz and low–pass filtered at 2 kHz. Liquid junction potentials were left uncompensated. Schaffer collateral was stimulated at 0.1 Hz. AMPAR EPSC amplitudes were calculated by averaging ∼30 peaks of EPSCs at –70 mV. NMDAR EPSC amplitudes were calculated by measuring the amplitude of EPSCs 50 ms after the stimulation at +40 mV. To induce LTP, cells were held at 0 mV while stimulating Schaffer collateral at 0.66 Hz for 120 pulses. Recordings with access resistance change by more than 20% were discarded. All experiments and analysis were performed blinded.

Statistics

All the statistical tests were performed using MiniTab software (Minitab Inc.). All values were expressed as mean + s.e.m.. Mann–Whitney's test was used to compare statistical difference between any two groups. $P < 0.05$ was taken as statistically significant difference.

Supplementary Material

Refer to Web version on PubMed Central for supplementary material.

Acknowledgement

We would like to thank Min Dai in the Monoclonal Antibody Core Facility of the Johns Hopkins University School of Medicine Department of Neuroscience for generating the monoclonal anti–GluR1 N–terminus antibody; Monica Coulter, Richard Johnson, and Yilin Yu in the Huganir Lab for their outstanding technical assistance; Bryan Bowman and Dr. Ruth M.E. Chalmers–Redman from Carl Zeiss Micro–Imaging Group for their excellent technical support. This work is funded by NIH grant R01NS036715 and the Howard Hughes Medical Institute.

References

1. Dingledine R, Borges K, Bowie D, Traynelis SF. The glutamate receptor ion channels. Pharmacol Rev. 1999; 51:7–61. [PubMed: 10049997]
2. Hollmann M, Heinemann S. Cloned glutamate receptors. Annu Rev Neurosci. 1994; 17:31–108. [PubMed: 8210177]
3. Shepherd JD, Huganir RL. The cell biology of synaptic plasticity: AMPA receptor trafficking. Annu Rev Cell Dev Biol. 2007; 23:613–643. [PubMed: 17506699]
4. Shi S, Hayashi Y, Esteban JA, Malinow R. Subunit-specific rules governing AMPA receptor trafficking to synapses in hippocampal pyramidal neurons. Cell. 2001; 105:331–343. [PubMed: 11348590]
5. Hayashi Y, et al. Driving AMPA receptors into synapses by LTP and CaMKII: requirement for GluR1 and PDZ domain interaction. Science. 2000; 287:2262–2267. [PubMed: 10731148]
6. Park M, Penick EC, Edwards JG, Kauer JA, Ehlers MD. Recycling endosomes supply AMPA receptors for LTP. Science. 2004; 305:1972–1975. [PubMed: 15448273]
7. Kim CH, Lisman JE. A role of actin filament in synaptic transmission and long-term potentiation. J Neurosci. 1999; 19:4314–4324. [PubMed: 10341235]
8. Krucker T, Siggins GR, Halpain S. Dynamic actin filaments are required for stable long-term potentiation (LTP) in area CA1 of the hippocampus. Proc Natl Acad Sci U S A. 2000; 97:6856–6861. [PubMed: 10823894]
9. Zhou Q, Xiao M, Nicoll RA. Contribution of cytoskeleton to the internalization of AMPA receptors. Proc Natl Acad Sci U S A. 2001; 98:1261–1266. [PubMed: 11158627]
10. Diakowski W, Grzybek M, Sikorski AF. Protein 4.1, a component of the erythrocyte membrane skeleton and its related homologue proteins forming the protein 4.1/FERM superfamily. Folia Histochem Cytobiol. 2006; 44:231–248. [PubMed: 17219717]
11. Hoover KB, Bryant PJ. The genetics of the protein 4.1 family: organizers of the membrane and cytoskeleton. Curr Opin Cell Biol. 2000; 12:229–234. [PubMed: 10712924]
12. Chen K, Merino C, Sigrist SJ, Featherstone DE. The 4.1 protein coracle mediates subunit-selective anchoring of Drosophila glutamate receptors to the postsynaptic actin cytoskeleton. J Neurosci. 2005; 25:6667–6675. [PubMed: 16014728]
13. Walensky LD, et al. A novel neuron-enriched homolog of the erythrocyte membrane cytoskeletal protein 4.1. J Neurosci. 1999; 19:6457–6467. [PubMed: 10414974]
14. Coleman SK, Cai C, Mottershead DG, Haapalahti JP, Keinanen K. Surface expression of GluR-D AMPA receptor is dependent on an interaction between its C-terminal domain and a 4.1 protein. J Neurosci. 2003; 23:798–806. [PubMed: 12574408]
15. Shen L, Liang F, Walensky LD, Huganir RL. Regulation of AMPA receptor GluR1 subunit surface expression by a 4. 1N-linked actin cytoskeletal association. J Neurosci. 2000; 20:7932–7940. [PubMed: 11050113]
16. Ashby MC, et al. Removal of AMPA receptors (AMPARs) from synapses is preceded by transient endocytosis of extrasynaptic AMPARs. J Neurosci. 2004; 24:5172–5176. [PubMed: 15175386]

17. Sekine-Aizawa Y, Huganir RL. Imaging of receptor trafficking by using alpha-bungarotoxin-binding-site-tagged receptors. Proc Natl Acad Sci U S A. 2004; 101:17114–17119. [PubMed: 15563595]
18. Thomas GM, Lin DT, Nuriya M, Huganir RL. Rapid and bi-directional regulation of AMPA receptor phosphorylation and trafficking by JNK. Embo J. 2008
19. Lin DT, Huganir RL. PICK1 and phosphorylation of the glutamate receptor 2 (GluR2) AMPA receptor subunit regulates GluR2 recycling after NMDA receptor-induced internalization. J Neurosci. 2007; 27:13903–13908. [PubMed: 18077702]
20. Ashby MC, Maier SR, Nishimune A, Henley JM. Lateral diffusion drives constitutive exchange of AMPA receptors at dendritic spines and is regulated by spine morphology. J Neurosci. 2006; 26:7046–7055. [PubMed: 16807334]
21. Kopec CD, Li B, Wei W, Boehm J, Malinow R. Glutamate receptor exocytosis and spine enlargement during chemically induced long-term potentiation. J Neurosci. 2006; 26:2000–2009. [PubMed: 16481433]
22. Heine M, et al. Surface mobility of postsynaptic AMPARs tunes synaptic transmission. Science. 2008; 320:201–205. [PubMed: 18403705]
23. Ehlers MD, Heine M, Groc L, Lee MC, Choquet D. Diffusional trapping of GluR1 AMPA receptors by input-specific synaptic activity. Neuron. 2007; 54:447–460. [PubMed: 17481397]
24. Bats C, Groc L, Choquet D. The interaction between Stargazin and PSD-95 regulates AMPA receptor surface trafficking. Neuron. 2007; 53:719–734. [PubMed: 17329211]
25. Groc L, et al. Differential activity-dependent regulation of the lateral mobilities of AMPA and NMDA receptors. Nat Neurosci. 2004; 7:695–696. [PubMed: 15208630]
26. Groc L, Choquet D, Chaouloff F. The stress hormone corticosterone conditions AMPAR surface trafficking and synaptic potentiation. Nat Neurosci. 2008; 11:868–870. [PubMed: 18622402]
27. Tardin C, Cognet L, Bats C, Lounis B, Choquet D. Direct imaging of lateral movements of AMPA receptors inside synapses. Embo J. 2003; 22:4656–4665. [PubMed: 12970178]
28. Borgdorff AJ, Choquet D. Regulation of AMPA receptor lateral movements. Nature. 2002; 417:649–653. [PubMed: 12050666]
29. Miesenbock G, De Angelis DA, Rothman JE. Visualizing secretion and synaptic transmission with pH-sensitive green fluorescent proteins. Nature. 1998; 394:192–195. [PubMed: 9671304]
30. Song I, Huganir RL. Regulation of AMPA receptors during synaptic plasticity. Trends Neurosci. 2002; 25:578–588. [PubMed: 12392933]
31. Boehm J, et al. Synaptic incorporation of AMPA receptors during LTP is controlled by a PKC phosphorylation site on GluR1. Neuron. 2006; 51:213–225. [PubMed: 16846856]
32. Hayashi T, Rumbaugh G, Huganir RL. Differential regulation of AMPA receptor subunit trafficking by palmitoylation of two distinct sites. Neuron. 2005; 47:709–723. [PubMed: 16129400]
33. Wozny C, et al. The function of glutamatergic synapses is not perturbed by severe knockdown of 4.1N and 4.1G expression. J Cell Sci. 2009; 122:735–744. [PubMed: 19225127]
34. Yudowski GA, et al. Real-time imaging of discrete exocytic events mediating surface delivery of AMPA receptors. J Neurosci. 2007; 27:11112–11121. [PubMed: 17928453]
35. Gardner SM, et al. Calcium-permeable AMPA receptor plasticity is mediated by subunit-specific interactions with PICK1 and NSF. Neuron. 2005; 45:903–915. [PubMed: 15797551]
36. Liu SJ, Cull-Candy SG. Subunit interaction with PICK and GRIP controls Ca2+ permeability of AMPARs at cerebellar synapses. Nat Neurosci. 2005; 8:768–775. [PubMed: 15895086]
37. Man HY, Sekine-Aizawa Y, Huganir RL. Regulation of {alpha}-amino-3-hydroxy-5-methyl-4-isoxazolepropionic acid receptor trafficking through PKA phosphorylation of the Glu receptor 1 subunit. Proc Natl Acad Sci U S A. 2007; 104:3579–3584. [PubMed: 17360685]
38. Steinberg JP, et al. Targeted in vivo mutations of the AMPA receptor subunit GluR2 and its interacting protein PICK1 eliminate cerebellar long-term depression. Neuron. 2006; 49:845–860. [PubMed: 16543133]
39. Lee HK, et al. Phosphorylation of the AMPA receptor GluR1 subunit is required for synaptic plasticity and retention of spatial memory. Cell. 2003; 112:631–643. [PubMed: 12628184]

40. Chung HJ, Steinberg JP, Huganir RL, Linden DJ. Requirement of AMPA receptor GluR2 phosphorylation for cerebellar long-term depression. Science. 2003; 300:1751–1755. [PubMed: 12805550]
41. Xia J, Chung HJ, Wihler C, Huganir RL, Linden DJ. Cerebellar long-term depression requires PKC-regulated interactions between GluR2/3 and PDZ domain-containing proteins. Neuron. 2000; 28:499–510. [PubMed: 11144359]
42. Lee HK, Barbarosie M, Kameyama K, Bear MF, Huganir RL. Regulation of distinct AMPA receptor phosphorylation sites during bidirectional synaptic plasticity. Nature. 2000; 405:955–959. [PubMed: 10879537]
43. Chung HJ, Xia J, Scannevin RH, Zhang X, Huganir RL. Phosphorylation of the AMPA receptor subunit GluR2 differentially regulates its interaction with PDZ domain-containing proteins. J Neurosci. 2000; 20:7258–7267. [PubMed: 11007883]
44. Kang R, et al. Neural palmitoyl-proteomics reveals dynamic synaptic palmitoylation. Nature. 2008; 456:904–909. [PubMed: 19092927]
45. Huang K, El-Husseini A. Modulation of neuronal protein trafficking and function by palmitoylation. Curr Opin Neurobiol. 2005; 15:527–535. [PubMed: 16125924]
46. Washbourne P. Greasing transmission: palmitoylation at the synapse. Neuron. 2004; 44:901–902. [PubMed: 15603731]
47. Rathenberg J, Kittler JT, Moss SJ. Palmitoylation regulates the clustering and cell surface stability of GABAA receptors. Mol Cell Neurosci. 2004; 26:251–257. [PubMed: 15207850]
48. El-Husseini Ael D, et al. Synaptic strength regulated by palmitate cycling on PSD-95. Cell. 2002; 108:849–863. [PubMed: 11955437]
49. DeSouza S, Fu J, States BA, Ziff EB. Differential palmitoylation directs the AMPA receptor-binding protein ABP to spines or to intracellular clusters. J Neurosci. 2002; 22:3493–3503. [PubMed: 11978826]
50. Moffett S, et al. Palmitoylated cysteine 341 modulates phosphorylation of the beta2-adrenergic receptor by the cAMP-dependent protein kinase. J Biol Chem. 1996; 271:21490–21497. [PubMed: 8702933]

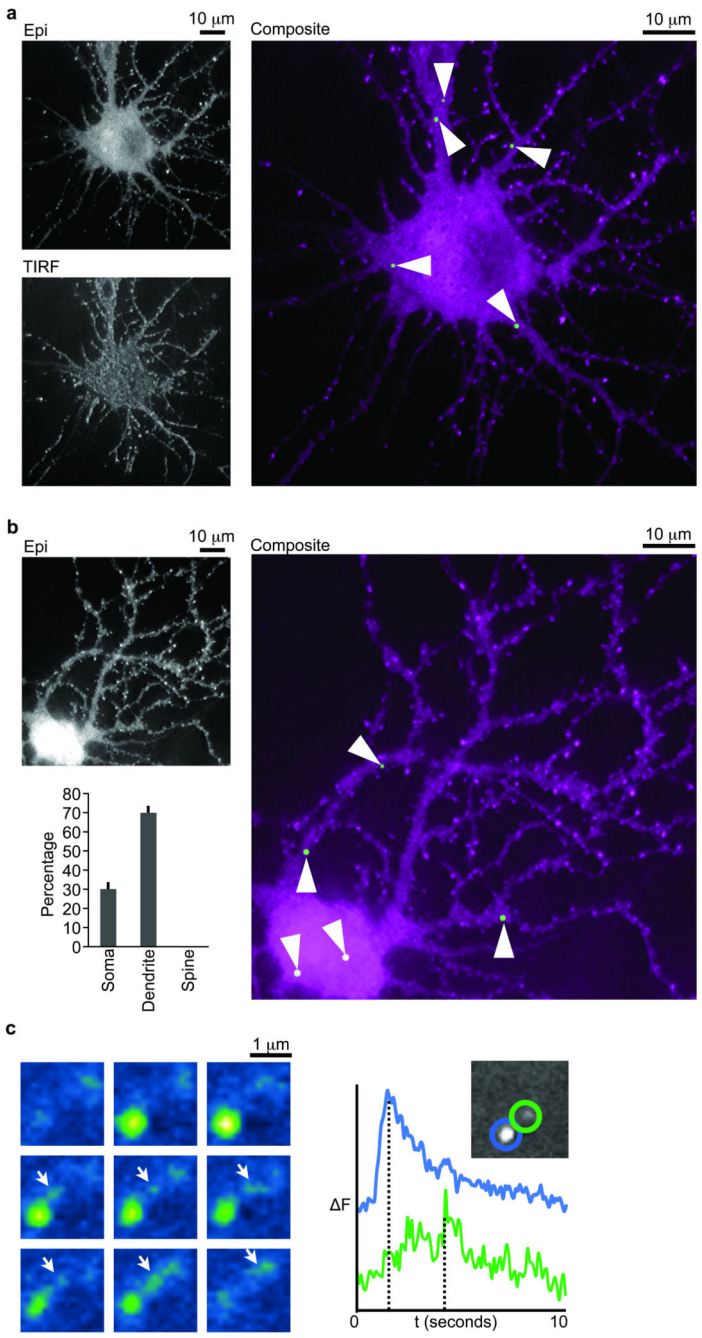

Figure 1.

Direct observation of GluR1 insertion events at extrasynaptic sites. **a)**. R1pH insertion observed under TIRF imaging mode. Upper left image: R1pH under epi–fluorescent mode; Lower left image: same neuron observed under TIRF mode; Right image: composite image (see Methods) of the same neuron (Magenta channel) with R1pH insertion sites (green spots indicated by white arrow heads) accumulated after 1 minute of observation. Scale bar: 10 μm. **b)**. R1pH insertion observed using epi–fluorescent imaging. Left image: a representative neuron expressing R1pH; Right image: composite image of the same neuron

(Magenta channel) with R1pH insertion sites (green spots indicated by white arrow heads) accumulated after 1 minute observation. Scale bar: 10 μm. Histogram on the lower left side: quantification of insertion distribution in percentage from total of 54 neurons, 204 insertion events: Soma: 30 ± 4 %; n = 54; Dendrite: 70 ± 4%, n = 54; Spine: 0%, n = 54. **c)**. Lateral diffusion of R1pH could be observed following insertion on the dendritic surface as indicated by the white arrowhead. Traces in right panel represent fluorescence changes over time. Blue trace was fluorescence change versus time in the center of insertion spot, as indicated by the blue circle in the image above the traces. Green trace was fluorescence change versus time in the green circle as indicated in the image above the traces. Dotted lines indicate the positions of fluorescence peak. Time between images shown was 400ms. Scale bar: 1 μm.

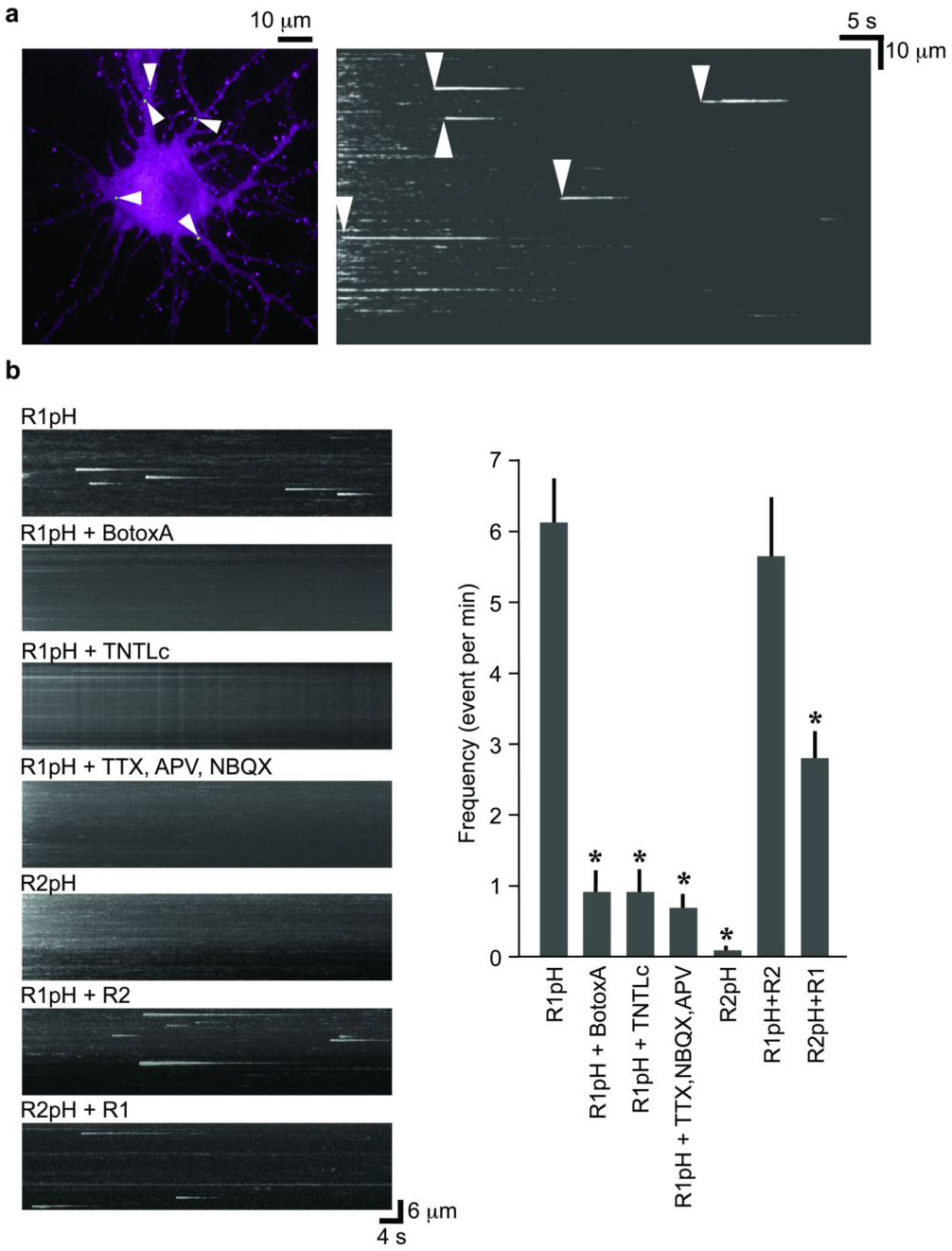

Figure 2.

Activity dependent GluR1 insertion. **a)**. Visualizing R1pH insertion in y–t maximum intensity projection images. Left panel: composite image of same neuron in Figure 1**a** (Magenta channel) with R1pH insertion sites (green spots indicated by white arrow heads); Right panel: y–t maximum intensity projection images (see Methods) of the same neuron, each “comet” like event as indicated by white arrow head with sudden rising and gradual decrease in fluorescence represents individual insertion event (also see supplemental Movie 2). **b)**. Representative y–t maximum intensity projection images of R1pH or R2pH insertion

under different conditions were on the left. Scale bar: 4 seconds / 6 μm. Quantification results of insertion frequency (event per min) were shown on the right histogram bar graph. R1pH: 6.1 ± 0.6, n = 51; R1pH + BotoxA: 0.9 ± 0.3, n = 20, $p < 0.0001$ (compared to R1pH unless otherwise specified); R1pH + TNTLc: 0.9 ± 0.3, n = 10, $p < 0.0001$; R1pH + TTX, NBQX, DL–APV: 0.7 ± 0.2, n = 20, $p < 0.0001$; R2pH: 0.1 ± 0.1, n = 37, $p < 0.0001$; R1pH + R2: 5.7 ± 0.8, n = 23, $p = 0.8675$; R2pH + R1: 2.8 ± 0.4, n = 20, $p < 0.0001$ compared to R2pH. Asterisk (*) indicates statistical significance.

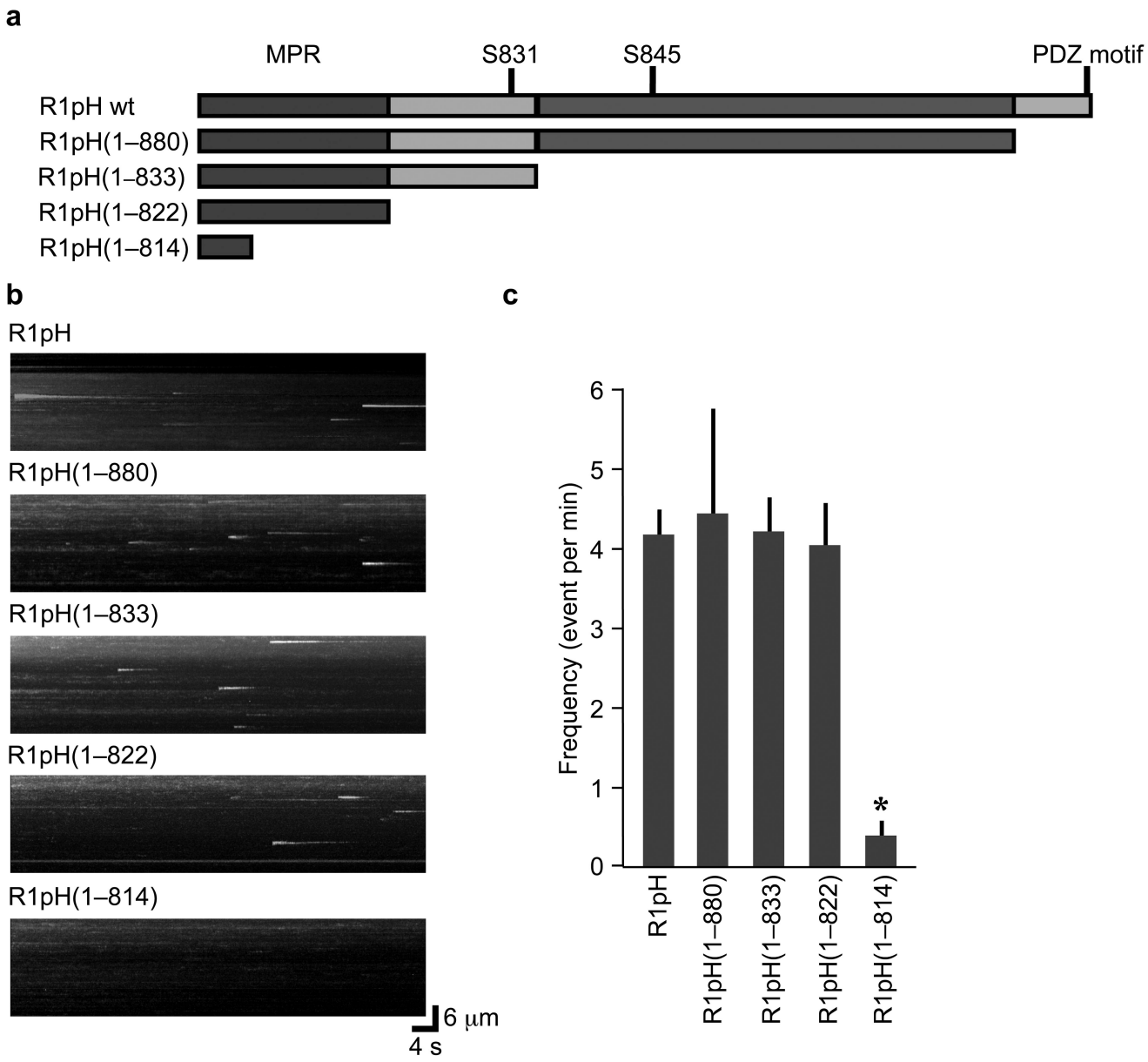

Figure 3.

GluR1 MPR is required for GluR1 insertion. **a)**. Schematic domain structure of GluR1 C–terminus demonstrating the serial C–terminal deletion constructs of R1pH. PDZ motif: the PDZ ligand at the end of GluR1 C–terminus; S845: Serine 845 of GluR1; S831: Serine 831 of GluR1; MPR: the membrane proximal region of GluR1 C–terminus. **b)**. Representative y–t maximum intensity projection images of insertion for different GluR1 deletion constructs. Scale bar: 4 seconds / 6 μm. **c)**. Statistical results of **b)**. The insertion frequency (event per min) of individual groups were as following: R1pH: 4.6 ± 0.3, n = 77; R1pH(1–880): 4.2 ± 1.0, n = 12, p = 0.1212 (compared to R1pH unless otherwise specified); R1pH(1–833): 4.2 ± 0.4, n = 23, p = 0.3863; R1pH(1–822): 4.0 ± 0.5, n = 28, p = 0.1493; R1pH(1–814): 0.4 ± 0.2, n = 25, p < 0.0001. Asterisk (*) indicates statistical significance.

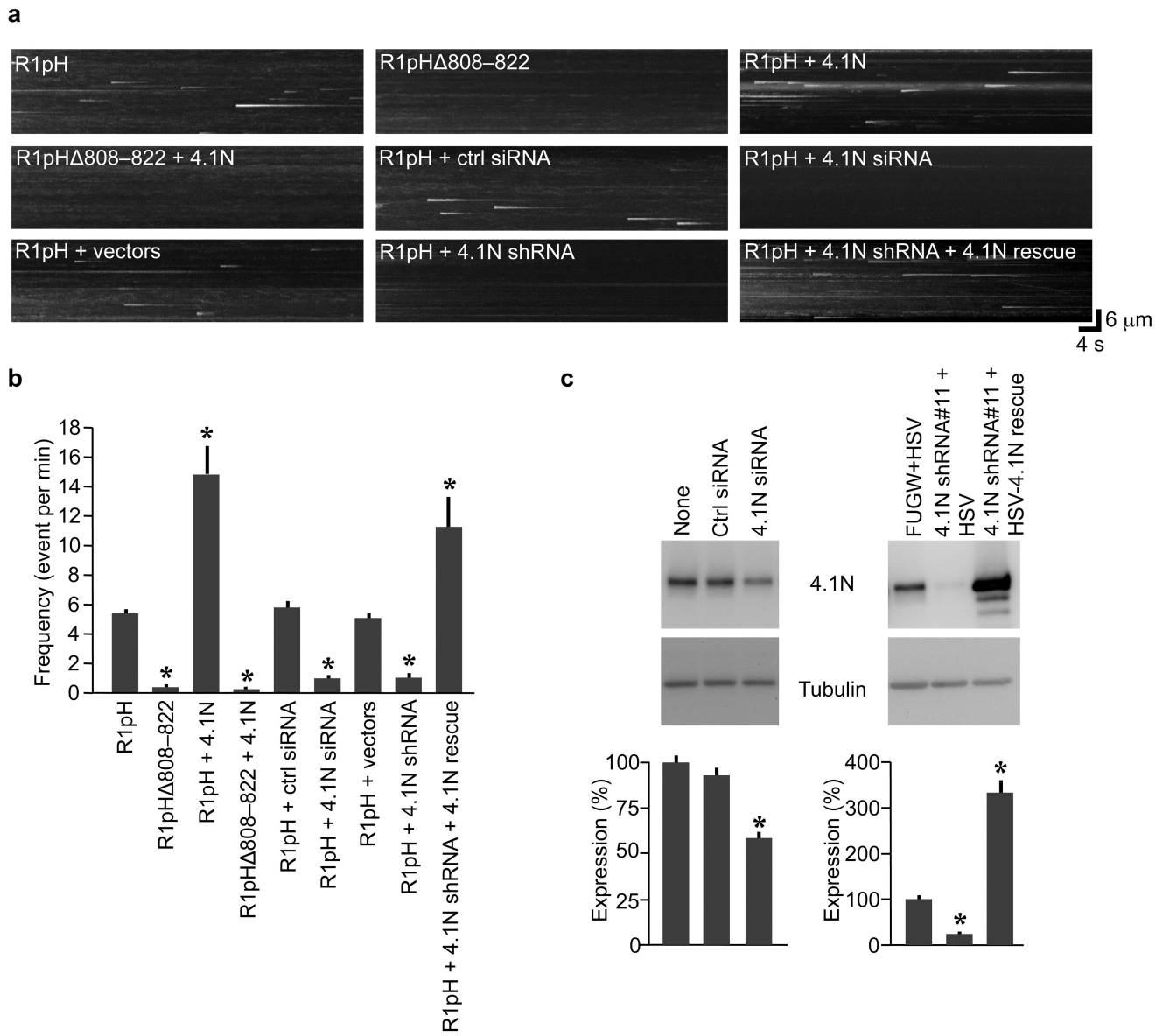

Figure 4.

4.1N is required for GluR1 insertion. **a)**. Representative y–t maximum intensity projection images for the indicated experimental groups. Scale bar: 4 seconds, 6 μm. **b)**. Statistical results for **a)**. Asterisk (*) indicates statistical significance (compared to R1pH unless otherwise specified). The insertion frequency (event per min) was: R1pH: 5.4 ± 0.2, n = 81; R1pHΔ808–822: 0.4 ± 0.1, n = 27, $p < 0.0001$; R1pH + 4.1N: 14.8 ± 1.9, n = 23, $p < 0.0001$; R1pHΔ808–822+4.1N: 1.1 ± 0.3, n = 20, $p = 0.09$ compared to R1pHΔ808–822. Ctrl siRNA: 5.8 ± 0.4, n = 20; 4.1N siRNA: 1.0 ± 0.2, n = 20, $p < 0.0001$ compared to Ctrl siRNA. R1pH + Vectors: 5.1 ± 0.3, n = 27; R1pH + 4.1NshRNA#11: 1.0 ± 0.3, n = 23, $p < 0.0001$ compared to R1pH + Vectors; R1pH + 4.1NshRNA#11 + 4.1Nrescue: 11.3 ± 2.0, n = 11, $p < 0.0001$ compared to R1pH + 4.1NshRNA#11. **c)**. Western Blot of 4.1N expression. Left panels: siRNA transfection. histogram: None (non–transfected): 100% (normalized to

tubulin), n = 3; Ctrl siRNA: 93 ± 3%, n = 3; 4.1N siRNA: 59 ± 3%, n = 3, $p < 0.05$ compared to Ctrl siRNA. Right panels: virus infection. histogram: FUGW + HSV: empty viruses as control (100%, n = 3); 4.1N shRNA#11 + HSV: 24 ± 3%, $p < 0.05$, n=3; 4.1N shRNA#11 + HSV–4.1N rescue: 333 ± 26%, $p < 0.05$, n = 3.

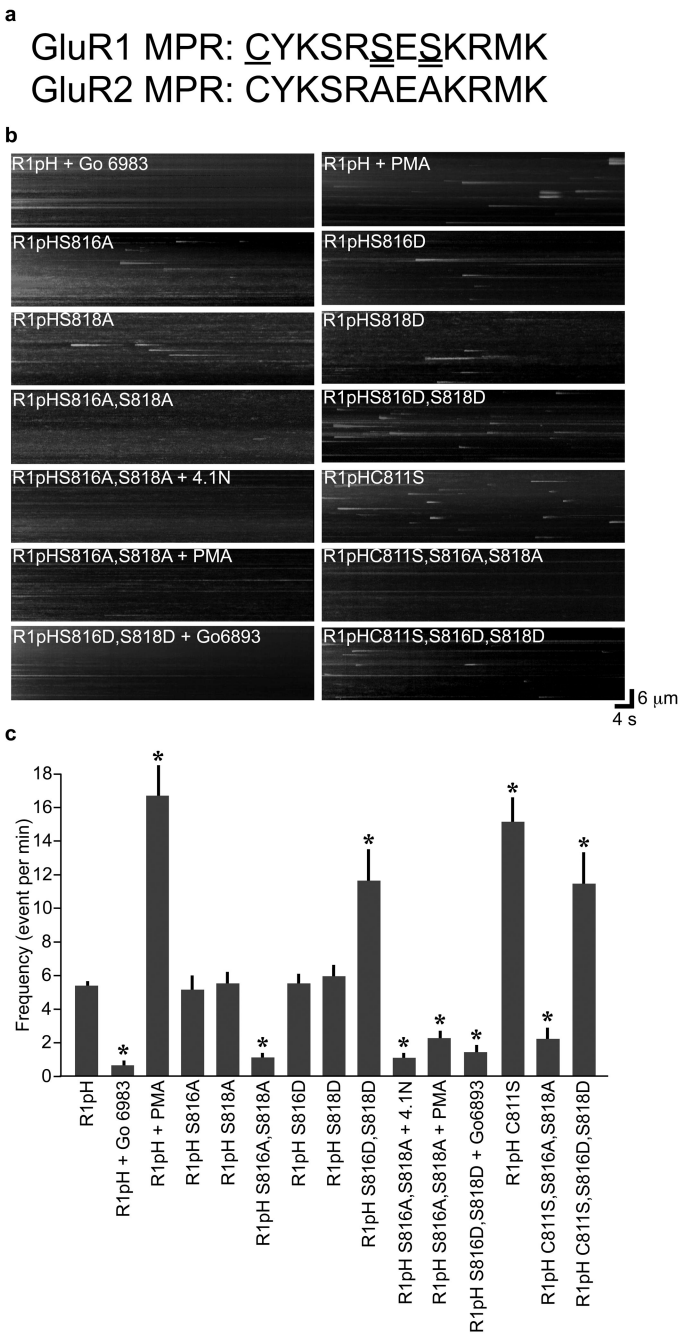

Figure 5.

Phosphorylation and de–palmitoylation regulate GluR1 insertion. **a)**. Sequence comparison between the MPR of GluR1 and GluR2. Double underline emphasized S816 and S818 of GluR1. C811 was marked with single underline. **b)**. Representative y–t maximum intensity projection images for the indicated experimental groups. Scale bar: 4 seconds, 6 μm. **c)**. Statistical results for **b)**. Asterisk (*) indicates statistical significance (compared to R1pH unless otherwise specified). The insertion frequency (event per min) was: R1pH: 5.3 ± 0.2, n = 95; Go 6983: 0.6 ± 0.3, n = 16; $p < 0.0001$; PMA: 16.6 ± 1.8, n = 20, $p < 0.0001$;

R1pHS816A: 5.2 ± 0.8, n = 25, p = 0.4279; R1pHS818A: 5.5 ± 0.7, n = 22, p = 0.9274; R1pHS816A,S818A: 1.1 ± 0.2, n = 30, p < 0.0001; R1pHS816D: 5.5 ± 0.5, n = 25, p = 0.7157; R1pHS818D: 6.0 ± 0.6, n = 20, p = 0.2674; R1pHS816D,S818D: 12.8 ± 1.3, n = 22, p < 0.0001; R1pHS816A,S818A + 4.1N: 1.1 ± 0.3, n = 20, p < 0.0001 compared to R1pH +4.1N; R1pHS816A,S818A + PMA: 2.3 ± 0.4, n = 18, p < 0.0001 compared to R1pH +PMA. R1pHS816D,S818D + Go 6983: 1.4 ± 0.4, n = 14, p < 0.0001 compared to R1pHS816D,S818D; R1pHC811S: 15.2 ± 1.4, n = 20, p < 0.0001; R1pHC811S,S816A,S818A: 2.2 ± 0.6, n = 22, p < 0.0001 compared to R1pHC811S; R1pHC811S,S816D,S818D: 12.2 ± 1.0, n = 22, p = 0.1116 compared to R1pHC811S.

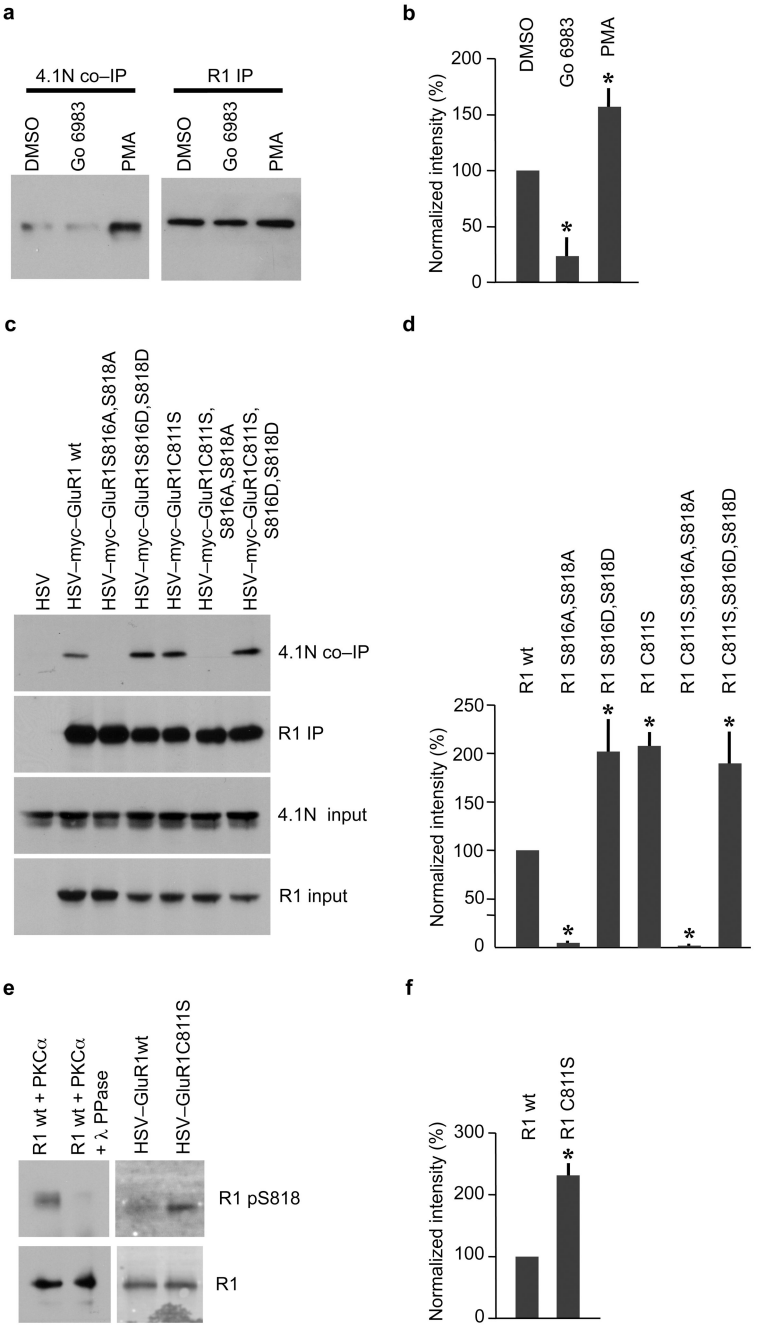

Figure 6.

Regulation of 4.1N and GluR1 interaction. **a)**. PKC inhibitor Go6983 inhibited and PKC activator PMA enhanced 4.1N and GluR1 interaction. **b)**. Quantification of **a)**. 4.1N co–IP intensity normalized to GluR1 IP was: DMSO: 100%, n = 3; Go 6983: 23 ± 16%, n = 3, $p < 0.05$; PMA: 157 ± 17%, n = 3, $p < 0.05$. **c)**. 4.1N co-IP with indicated GluR1 mutants. From top to bottom, the 4 panels represented: co–IP of 4.1N with myc–GluR1; myc–GluR1 IP; 4.1N input; myc–GluR1 input. **d)**. Quantification of **c)**. 4.1N co–IP intensity normalized to myc–GluR1 IP (compared to R1wt) was: R1wt: 100%, n = 3; GluR1S816A,S818A: 2 ± 3%,

n = 3, p < 0.05; GluR1S816D,S818D: 202 ± 33%, n = 3, p < 0.05; GluR1C811S: 209 ± 14%, n = 3, p < 0.05; GluR1C811S,S816A,S818A: 4 ± 7%, n = 3, p < 0.05; GluR1C811S,S816D,S818D: 189 ± 32%, n = 3, p < 0.05. **e)**. De–palmitoylation of GluR1C811 enhanced PKC phosphorylation of S818. Left panels: anti–R1 phospho–S818 is phospho–specific. Right panels: phospho–S818 of GluR1wt or GluR1C811S in GluR1 knockout neurons treated with PMA for 30 minutes. **f)**. Quantification of GluR1S818 phosphorylation normalized to GluR1 IP, GluR1wt: 100%, n = 3; R1C811S: 232 ± 19%, n = 3, p < 0.05. Asterisk (*) indicates statistical significance.

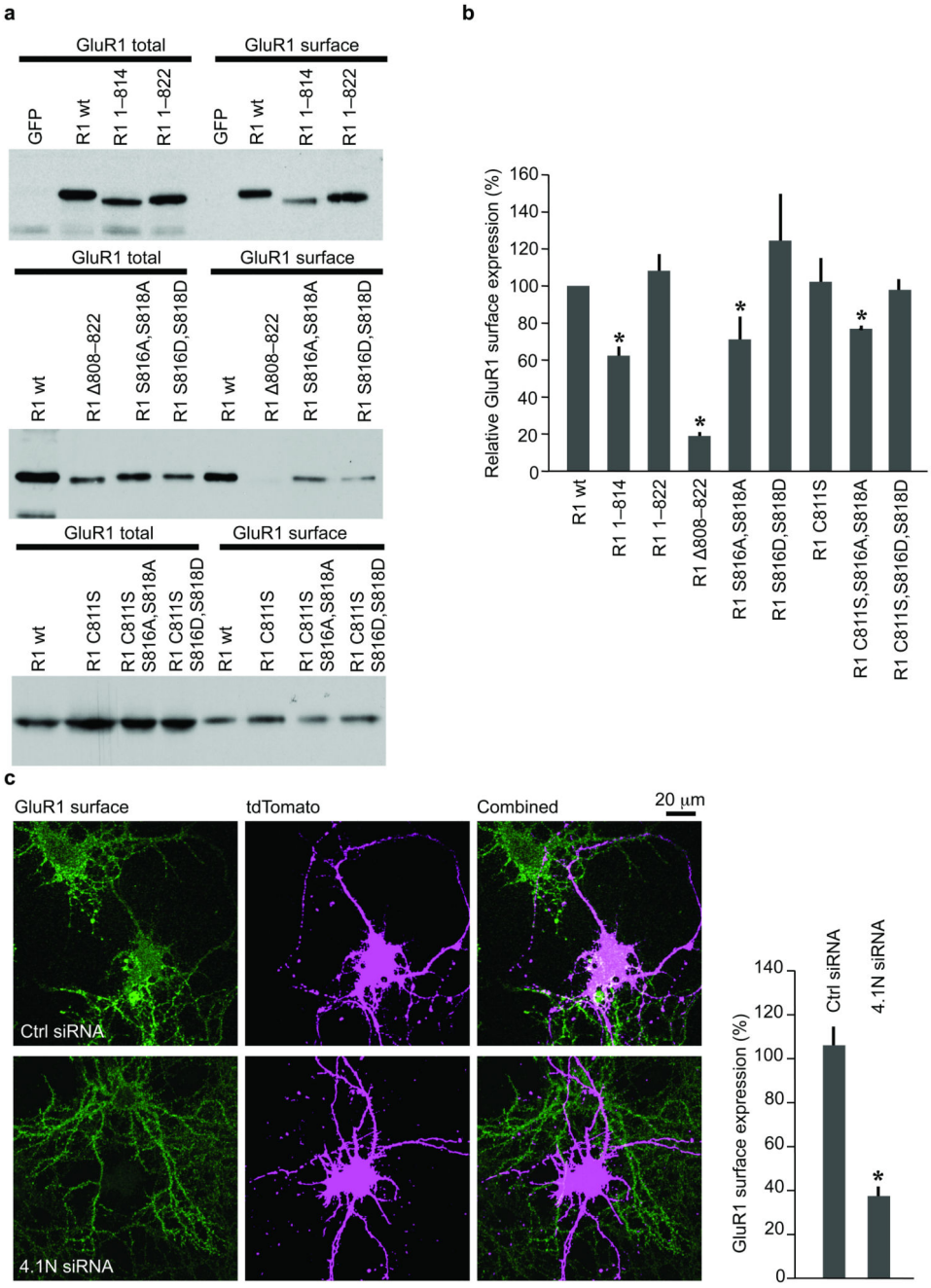

Figure 7.

Reduction in GluR1 insertion results in reduced surface expression. **a)**. Western blots of Biotinylation experiments to detect surface expression of different GluR1 mutants. **b)**. Quantification of **a)**. Surface/Total ratio (compared to GluR1wt) was: GluR1wt: 100%, n = 12; GluR1(1–814): 62 ± 5%, n = 6, $p < 0.05$; GluR1(1–822): 108 ± 9%, n = 6, $p = 1.00$; GluR1 Δ808–822: 19 ± 0.4%, $p < 0.05$; GluR1S816A,S818A: 71 ± 12%, n = 3, $p < 0.05$; GluR1S816D,S818D: 124 ± 25%, n = 3, $p = 0.5169$; GluR1C811S: 102 ± 13%, n = 3, $p = 0.5169$; GluR1C811S,S816A,S818A: 77 ± 1%, n = 3, $p < 0.05$;

GluR1C811S,S816D,S818D: 97 ± 5%, n = 3, p = 0.5169. **c)**. Surface expression level of endogenous GluR1 containing AMPARs was reduced when 4.1N expression was knocked down by siRNA. Left panels (green): surface expression level of endogenous GluR1; central panels (Magenta): tdTomato labeling transfected neurons; right panels combine GluR1 antibody labeling fluorescent images with tdTomato fluorescence. The total fluorescence intensities from siRNA transfected neurons was normalized to that of neighboring non–transfected neurons as 100%. The surface expression level of neurons transfected with Control siRNA + tdTomato was 106 ± 8%, n = 20, that of neurons transfected with 4.1N siRNA + tdTomato was 37 ± 4%, n = 22, $p < 0.0001$. Asterisk (*) indicates statistical significance.

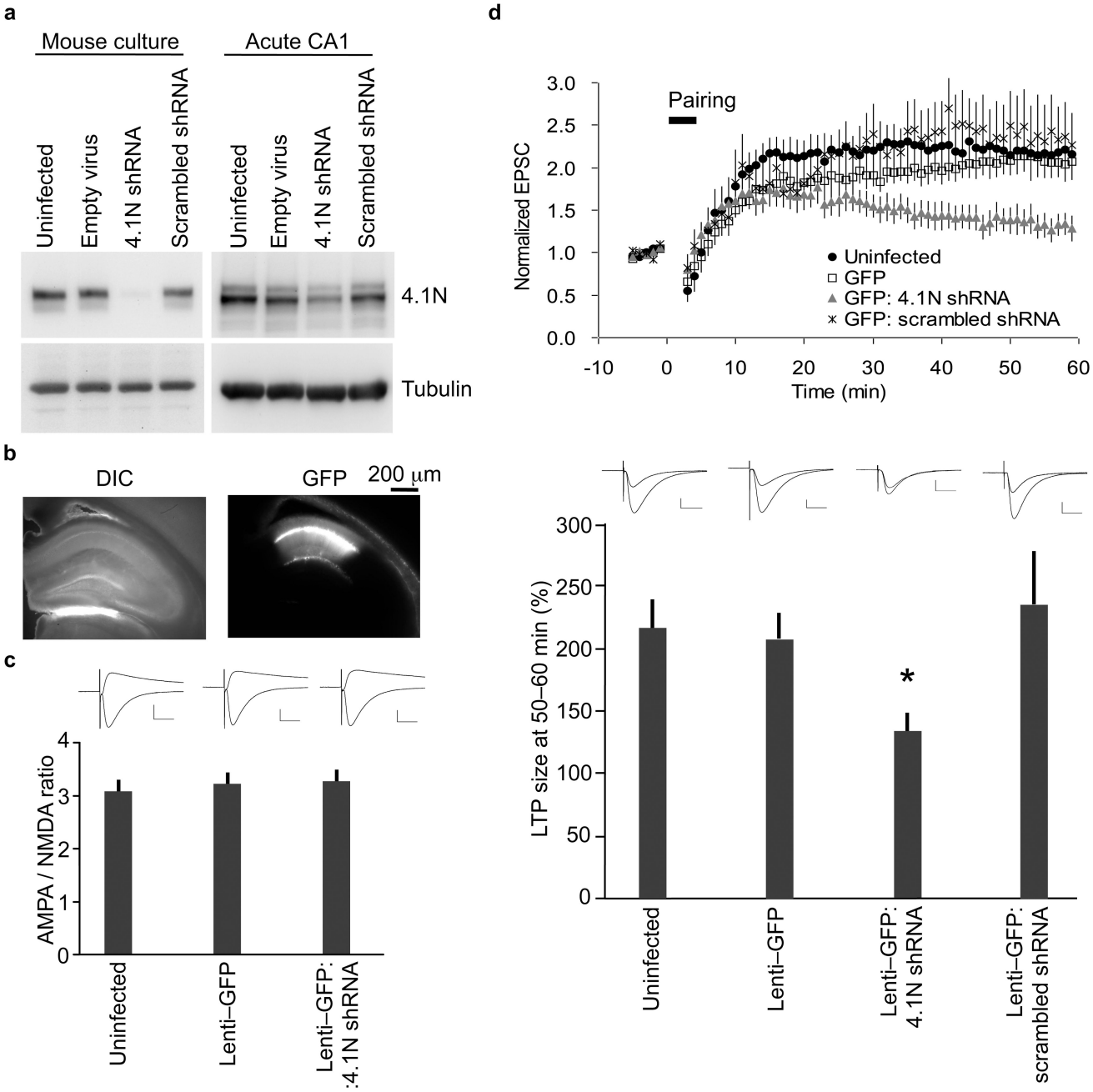

Figure 8.

4.1N is required for LTP expression in acute hippocampal slices of adult mice. **a)**. Western blots showing knock–down of 4.1N by infecting mouse cortical culture *in vitro* or hippocampal CA1 region *in vivo* with lentiviral 4.1N shRNA. **b)**. Representative images of mouse hippocampal slices infected *in vivo* with lentivirus, scale bar: 200 μm GFP. **c)**. AMPA/NMDA ratio measured at Schaffer collateral – CA1 synapses of uninfected (3.1 ± 0.2, n = 20), GFP–infected (3.2 ± 0.2, n = 27), and GFP:4.1N shRNA–infected (3.3 ± 0.2, n = 17) cells. Representative EPSC traces at −70 mV (negative current) and +40 mV (positive current) are shown for each condition above the bar graph (scale bars: 20 ms / 100 pA). **d)**.

LTP of uninfected, GFP–infected, GFP: 4.1N shRNA–infected, and GFP:scrambled shRNA–infected cells. Representative EPSC traces during baseline period and 50–60 min after LTP induction were shown for each condition above the bar graph (scale bars: 20 ms / 50 pA). The EPSC amplitude at 50–60 minutes after the induction of LTP compared to the baseline period was defined as the size of LTP expression and quantified in lower histogram bar graph: uninfected: 218 ± 23%, n = 10; lenti–GFP: 208 ± 20%, n = 12; lenti–GFP:4.1N shRNA: 133 ± 15%, n = 11, $p < 0.05$ compared to any of the control groups; lenti–GFP:scrambled shRNA: 235 ± 43%, n = 11. Asterisk (*) indicates statistical significance.